Vortex glass transitions in disordered three-dimensional *XY* models: Simulations for several different sets of parameters

Peter Olsson
Department of Physics, Umeå University, 901 87 Umeå, Sweden
(Received 9 December 2004; revised manuscript received 2 September 2005; published 26 October 2005)

The anisotropic frustrated three-dimensional (3D) *XY* model with strong disorder in the coupling constants is studied as a model of a disordered superconductor in an applied magnetic field. Simulations with the exchange Monte Carlo method are performed for frustrations $f=1/5$ and $f=1/4$, corresponding to two different values of the magnetic field along the z direction. The anisotropy is also varied. The determination of the helicity modulus from twist histograms is discussed in some detail and the helicity modulus is used in finite size scaling analyses of the vortex glass transition. The general picture is that the behavior in [Phys. Rev. Lett. **91**, 077002 (2003)] is confirmed. For strong (e.g., isotropic) coupling in the z direction the helicity modulus fails to scale and it is argued that this is due to a too small effective randomness of such systems for the accessible system sizes.

DOI: 10.1103/PhysRevB.72.144525 PACS number(s): 74.25.Dw, 64.60.−i, 74.25.Qt

I. INTRODUCTION

An applied magnetic field in a type-II superconductor will give rise to vortex lines that penetrate the sample. A current applied perpendicular to these vortex lines will give rise to a force perpendicular to both the current and the magnetic field. In a pure system there is nothing that hinders the motion of the vortex lines and their motion leads to flux-flow resistivity and therefore a loss of superconductivity. The presence of point disorder could mean a substantial reduction of the mobility of the vortex lines, but the resistivity would, in the conventional picture, nevertheless always be nonzero.

A vortex glass phase is an alternative possibility that was suggested to restore the true superconducting state.[1,2] The idea is that the finite disorder strength together with the vortex line interaction leads to diverging energy barriers against the vortex motion, and thereby a vanishing resistivity. This was suggested to take place through a continuous transition with universal exponents and certain scaling properties. Experimental results in support of this picture have been reported,[3–5] but the conclusion of a vortex glass phase has also often been questioned.[6]

There has also been much work on simulations of vortex glass models. The simplest three-dimensional (3D) vortex glass model, which was also the first to be studied, is the 3D gauge glass model that includes the disorder through a random vector potential added to the phase difference of the superconducting order parameter. Already the early simulations[7,8] found strong evidence for a transition, and with the exchange Monte Carlo (MC) technique[9] it has been possible both to give more convincing evidence for a transition and to determine the value of the correlation length exponent to $\nu=1.39\pm0.04$.[10]

A problem with using the 3D gauge glass as a model of a disordered superconductor in an applied magnetic field, is the generally recognized fact that the model lacks some of the properties and symmetries of the physical system. The applied field both breaks the spatial symmetry of the system and introduces an additional length scale. In a model that properly includes these features one would, e.g., have the possibility of anisotropic scaling, i.e., different divergences of the correlations parallel and perpendicular to the applied field.

Several attempts have been made to simulate systems with the correct symmetry. An early paper was a study of the defect-wall energy at zero temperature for four different *XY*-like spin-glass models. This study, though limited to sizes $L\leqslant 5$, found evidence for another universality class.[11] The more recent studies make use of the exchange Monte Carlo method (see below). The first of these is from simulations of a frustrated 3D *XY* model with filling $f=1/4$ and disorder in the coupling constants.[12] The correlation length exponent was determined to be $\nu=2.2$ even though the quality of the data did not allow for any firm conclusions. In a second paper by the same author the open boundary conditions employed in the first study were changed to standard periodic boundary conditions.[13] The data now rather suggested $\nu\approx 1.1$, but some quantities still failed to provide good scaling. Some aspects of these simulations are discussed in Sec. VI.

Simulations have also been performed with vortex lines instead of the phase variables of the *XY* model.[14] A simulation study of such a vortex line model with strong point disorder gives the value $\nu=0.7$, indistinguishable from the 3D *XY* exponent.

The present paper is a sequel of Ref. 15 which gave the first numerical support for 3D gauge glass universality in vortex glass simulations with the correct symmetry. The approach there was to study an anisotropic model with much weaker couplings in the field direction than in the directions perpendicular to the field. This was a natural choice due to experiences from the first-order transition between the Abrikosov lattice and the vortex line liquid. In these simulations[16,17] it has been found that the correct behavior required a great flexibility of the field induced vortex lines, which could be obtained either with a very large size of the system along the direction of the applied field or with weaker couplings between the phase angles in the same direction. As

we will see below the choice of an anisotropic model turns out to be crucial for obtaining convincing scaling collapses.

Another recent study of the vortex glass transition has been done on a model that extends the elastic description of a vortex lattice to include dislocations.[18] The correlation length exponent of the transition was found to be $\nu \approx 1.3$, which within reasonable error bars also is consistent with 3D gauge glass universality.

In the present paper we present detailed analyses of the frustrated 3D *XY* model with strong disorder in the coupling constants. The paper is an extension of Ref. 15 in two respects; (i) The determination of the helicity modulus from simulations with twist fluctuations as well as analyses of the thermalization and the exchange steps in the Monte Carlo simulations are described in considerably more detail. (ii) Simulations and analyses have been done for several different sets of parameters.

The organization of the paper is as follows: In Sec. II we introduce the vortex glass model and the different sets of parameters used in the simulations and also briefly discuss the behavior at weak disorder. Section III deals with the determination of the helicity modulus from twist histograms. This is a rather technical section which may be skipped over at the first reading of the paper. In Sec. IV the simulation methods are discussed with emphasis on some aspects of the exchange Monte Carlo technique, and Sec. V gives the simulation results. Finally, Sec. VI contains a discussion together with a short summary.

II. THE VORTEX GLASS MODEL

The model we simulate is given by the Hamiltonian[15,19]

$$\mathcal{H} = -\sum_{\text{bonds } i\mu} J_{i\mu} \cos(\theta_i - \theta_{i+\hat{\mu}} - A_{i\mu} + \delta_\mu^{(\mathbf{r}_i \cdot \hat{\mu})}), \qquad (1)$$

where θ_i is the phase of the superconducting wave function at site i with position $\mathbf{r}_i$ of a periodic $L_x \times L_y \times L_z$ lattice, and the sum is over all bonds in directions $\mu = x, y, z$. The size in the x and y directions are the same; $L_x = L_y = L$. An applied magnetic field in the z direction is obtained through the quenched vector potential with the choice $A_{ix} = 2\pi f y_i$ and $A_{iy} = A_{iz} = 0$. The simulations are performed with fluctuating twist boundary conditions[20] which in the duality relation corresponds to a vortex line model with periodic boundary conditions. We make use of L_μ twist variables $\delta_\mu^{(\mathbf{r}_i \cdot \hat{\mu})}$ in each direction, and the total twists in the respective directions are $\Delta_\mu = \Sigma_{j=1}^{L_\mu} \delta_\mu^{(j)}$.[21] These variables are updated with the usual Metropolis method. We have run simulations for four different sets of parameters, summarized in Table I. The disorder is put in the coupling constants, which are chosen as

$$J_{i\mu} = J_\perp (1 + \varepsilon_{i\mu}), \quad \mu = x, y,$$

$$J_{iz} = J_\parallel (1 + \varepsilon_{i\mu}), \quad \text{only sets C and D.}$$

For set A (which is the one used in Ref. 15 the $\varepsilon_{i\mu}$ are independent variables from a Gaussian distribution with $\langle \varepsilon_{i\mu} \rangle = 0$ and $p = \sqrt{\langle \varepsilon_{i\mu} \rangle^2} = 0.40$. For sets B through D, $\varepsilon_{i\mu}$ are instead from a uniform distribution between -1 and 1. Another difference (as indicated in the Table) is that the disorder for sets A and B is only put on the couplings in the x and y directions whereas the sets C and D are also disordered along z. The reason for this choice is to facilitate a direct comparison with the simulations in Ref. 13.

TABLE I. Four different parameter sets have been simulated. Information about the runs are given in Table II.

Set	f	$J_\parallel/J_\perp$	Disorder	Directions
A	1/5	1/40	Gaussian	x,y
B	1/5	1/10	rectangular	x,y
C	1/4	1/10	rectangular	x,y,z
D	1/4	1	rectangular	x,y,z

The emphasis of this paper is the behavior of this model in the presence of strong disorder. To put this in its wider context we here briefly discuss the behavior of this model with *weak* disorder. In the pure model there is a low temperature phase where the vortex lines become straight and order into a vortex solid—the Abrikosov lattice. The phase diagram therefore consists of the three phases of vortex solid, vortex liquid, and vortex glass. A determination of the solid-liquid phase boundary for the more dilute system with $f = 1/20$ has been given in Ref. 19. A more complete examination of the phase diagram for $f = 1/5$ with the three phases, vortex solid, vortex liquid, and vortex glass, will be given elsewhere.[22]

To examine the vortex glass transition it is important to avoid entering into the vortex solid and that has been considered when choosing the parameters in Table I. The disorder strength for set A has been chosen as $p = 0.4$ which is well-separated from the vortex solid that melts at $p \approx 0.2$. As $J_\parallel$ increases, the tendency to form a vortex solid increases. For set B with $J_\parallel/J_\perp = 1/10$ this tendency was countered both by increasing the disorder strength and by increasing the aspect ratio to $L_z/L = 1$ instead of $L_z/L = 3/5$ or 2/5 used for set A. For isotropic systems with $f = 1/5$ the vortex solid seemed to be the stable phase but for $f = 1/4$ the tendency to form a vortex solid is weaker and we found, in agreement with Ref. 13, that the disorder was strong enough to destroy the vortex solid.

III. DETERMINATION OF THE HELICITY MODULUS

A way to determine the helicity modulus from twist histograms was introduced in Ref. 15. The presentation was rather short and the purpose with this section is to give a pedagogical and reasonably complete description of the method. The most important point is the origin of the bias towards too large values of the helicity modulus and the procedure to obtain unbiased values as described in Eq. (7).

For the discussion we start by considering the ordinary 3D *XY* model (no disorder and no frustration), which is defined by the Hamiltonian

$$H = \sum_{\langle ij \rangle} U(\theta_i - \theta_j).$$

A common choice for the spin interaction is $U(\phi) = -J \cos(\phi)$. The helicity modulus, which is the standard

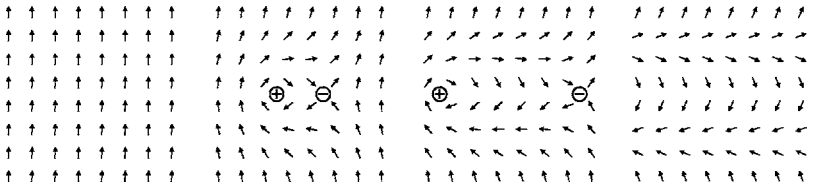

FIG. 1. The separation of a vortex pair in a system with periodic boundary conditions gives a configuration with the phase rotating by 2π.

probe of phase coherence in XY models, is defined through the response of the system to an applied twist. One way to define the twist is to generalize the standard periodic boundary conditions $\theta_{(L,0,0)}=\theta_{(0,0,0)}$ to

$$\theta_{(L,0,0)} = \theta_{(0,0,0)} + \Delta_x,$$

and similarly in the other directions. Here Δ_x is the phase mismatch or the *total twist* in the x direction. One may alternatively think about the twist as being spread out across the whole system and introduce the *twist per link*, $\delta_\mu=\Delta_\mu/L_\mu$. The Hamiltonian may then be written

$$H = \sum_i \sum_\mu U(\theta_{i+\mu} - \theta_i - \delta_\mu).$$

The helicity modulus is defined through the change in the free energy $F(\Delta_\mu)$, or the free energy per site $f=F/V$, as

$$\Upsilon_\mu = \left.\frac{\partial^2 f}{\partial \delta_\mu^2}\right|_{\delta_\mu=0} = \frac{L_\mu^2}{V}\left.\frac{\partial^2 F}{\partial \Delta_\mu^2}\right|_{\Delta_\mu=0}, \tag{2}$$

which gives the correlation function,[23]

$$\Upsilon_\mu = \frac{1}{V}\left\langle \sum_i U''(\phi_{i\mu})\right\rangle - \frac{1}{TV}\left\langle \left(\sum_i U'(\phi_{i\mu})\right)^2\right\rangle. \tag{3}$$

With this correlation function the determination of the helicity modulus is done in simulations performed with zero twist. Note that the derivative in Eq. (3) is evaluated at the minimum of the free energy which typically is $\Delta=0$. However, in some disordered models there is nothing that guarantees that the minimum of the free energy is at zero twist. The approach taken here is to study such systems with simulations that include the twist fluctuations as additional dynamical variables.

A. Twist fluctuations

There is a well-known duality relation between an XY model in the Villain representation and a gas of interacting charges. In two dimensions this is a Coulomb gas with logarithmic interactions and in three dimensions a gas of interacting loops. As observed by several authors[20,24–26] the XY model that is dual to a Coulomb gas with periodic boundary conditions also includes twist fluctuations. Physically, the twist fluctuations are necessary for the process when a pair of vortices separate, cross the boundary, and recombine. In the absence of twist fluctuations such a process gives a configuration where the phase rotates by 2π across the system in the direction perpendicular to the vortex separation, as illustrated in Fig. 1. The effect is that recombinations of vortices are effectively prohibited. Figure 2 illustrates the vortex separation in the presence of twist fluctuations in the y direction.

B. Basic relations

An alternative means to obtain Υ_μ is by first determining the free energy, $F(\Delta_\mu)$. The simulations are then performed with fluctuating twists in the μ direction and periodic boundary conditions in the other two directions,

$$H = \sum_{i,\lambda\neq\mu} U(\theta_{i+\lambda} - \theta_i) + \sum_i U(\theta_{i+\mu} - \theta_i + \Delta_\mu/L_\mu).$$

The free energy is obtained from the histogram $P(\Delta_\mu)$ through

$$F(\Delta_\mu) = -T \ln P(\Delta_\mu),$$

and the helicity modulus may be determined from a fit of the free energy in a narrow range r of Δ around zero. Dropping the index μ we write,

$$F(\Delta) = F_0 + \frac{1}{2}L\Upsilon\Delta^2, \quad |\Delta| < r. \tag{4}$$

This is trivial in principle, but some complications arise when this is applied to simulation data with limited accuracy. The following sections will discuss this question in some detail.

C. Range of Δ

Since Υ is defined as a derivative of the free energy, the range of Δ used for the fit to Eq. (4) should be chosen as small as possible. To check for the dependence of Υ on the

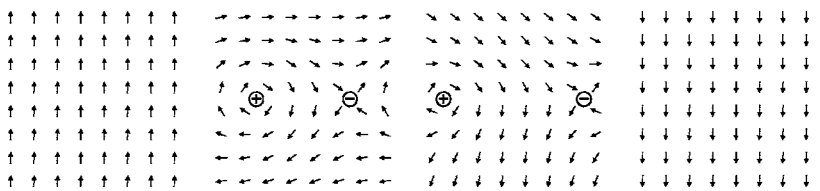

FIG. 2. The separation of a vortex pair in a system with fluctuating twist boundary conditions. The twist variable is here applied between the top and the bottom rows of spins that are connected through the boundary conditions. The four panels are for $\Delta_y=0,\pi,0.85\times2\pi$, and 2π, respectively.

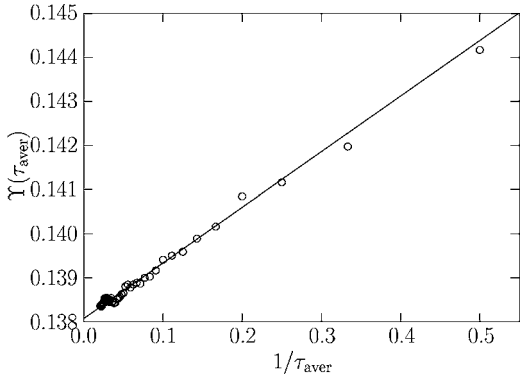

FIG. 3. When Υ is determined from Eq. (5) with Δ^0 as a free parameter, the obtained Υ becomes biased towards too large values. This bias decays with $1/\tau_{\rm aver}$, where $\tau_{\rm aver}$ is the number of bins used for collecting data, cf. Eq. (6). The data is obtained from an isotropic lattice with $L=8$ and $T=2.2$.

range r we made use of a twist histogram $P(\Delta)$ for an ordinary 3D XY model, with $L=8$ and $T=2.2$ close to T_c. It is then found that there is a strong dependence on r which to a good approximation is $\Upsilon(r)-\Upsilon(0)\sim -r^2$, due to the presence of a Δ^4 term in $F(\Delta)$. From $\Upsilon(r)$ for small r an extrapolation to $r=0$ gives $\Upsilon=0.1389(3)$ in excellent agreement with the more precise value, $\Upsilon=0.13\,899(8)$ obtained with Eq. (3) from a MC simulation with the Wolff cluster algorithm.[27]

D. Disordered systems: Unknown Δ^0

We have so far only been concerned with models with the known minimizing twist $\Delta^0=0$. The presence of disorder may however mean that the minimizing twist becomes different for different disorder realizations and is not known at the outset, and this turns out to add an unexpected complication to the analysis.

In the case when Δ^0 is unknown the analysis consists of two steps: (i) take some data from a certain range around the maximum of $P(\Delta)$ (the minimum of the free energy) and (ii) fit the free energy from this data to a second order polynomial in Δ to determine Υ. For this second step Eq. (4) has to be changed to

$$F(\Delta)=F_0+\frac{1}{2}L\Upsilon(\Delta-\Delta^0)^2, \quad |\Delta-\Delta^0|<r. \tag{5}$$

When used on simulation data, where statistical fluctuations are always present, this method happens to give values of the helicity modulus that are biased towards too large values.

To illustrate this fact we have again made use of twist histograms for the 3D XY model. Even though the minimizing twist is still zero we now take Δ^0 to be a free variable in the analysis. For the complete run, which consists of about 7000 bins, there is no discernible effect of the randomness, but by constructing twist histograms from $\tau_{\rm aver}$ (say 2–40) consecutive bins the effect becomes significant and may be systematically examined. The bin size is $2^{18}=262\,144$ sweeps across the system. Figure 3 shows $\Upsilon(\tau_{\rm aver})$ versus $1/\tau_{\rm aver}$. The values of these run-length dependent values $\Upsilon(\tau_{\rm aver})$ are based on close to 7000 different twist histograms constructed from $\tau_{\rm aver}$ consecutive bins

$$\bar{P}^{(i)}(\Delta;\tau_{\rm aver})=\frac{1}{\tau_{\rm aver}}\sum_{\tau=1}^{\tau_{\rm aver}}P(\Delta;i+\tau). \tag{6}$$

The message from this figure is that there is a bias in determinations of Υ that are based on too short runs. It is also clear that there is a $1/\tau_{\rm aver}$-dependence and the data may be extrapolated to $\Upsilon(\tau_{\rm aver}\to\infty)\approx 0.1381$. Since this data is obtained with a finite range, $r=0.0625$, this value should be compared to, and agrees well with, the corresponding value obtained in Sec. III C.

A clue to the origin of this bias is given by examining Δ^0, which is the location of the minimum of the free energy. Since the ground state for the pure 3D XY model is a state with zero twist, $\Delta^0=0$, the deviations from zero are due to the statistical fluctuations in the twist histograms. We find $\langle(\Delta^0)^2\rangle\sim 1/\tau_{\rm aver}$, which is the same as the behavior of an average $\bar{x}$ of N independent values x_i from a distribution with zero mean: $\langle\bar{x}^2\rangle\sim 1/N$.

The key observation is now that Υ as a measure of the curvature of the free energy is inversely related to the width of the distribution. For N samples x_i the width of the distribution is characterized by the variance and from elementary texts in statistics it is well known that $\sigma^2_{\rm naive}=1/N\Sigma_i(x_i-\bar{x})^2$ gives a biased estimate that may be corrected by

$$\sigma^2=\frac{N}{N-1}\sigma^2_{\rm naive}.$$

The well-known reason for this correction is the use of $\bar{x}$ instead of the true average of the distribution. In the analysis of the histogram data the location of Δ^0 is a similar source of error and it is natural to expect the same kind of effect in the analysis of the histogram data. With $\Upsilon(\tau_{\rm aver})$ and $\Upsilon(\infty)$ inversely related to $\sigma^2_{\rm naive}$ and σ^2, respectively, and the number of independent samples given by $N=\tau_{\rm aver}/b$, we obtain

$$\Upsilon(\tau_{\rm aver})=\frac{1}{1-b/\tau_{\rm aver}}\Upsilon(\infty). \tag{7}$$

Here b is a constant with dimension of time. The expression above may also be written

$$\frac{1}{\Upsilon(\tau_{\rm aver})}=\frac{1}{\Upsilon(\infty)}-b'/\tau_{\rm aver}, \tag{8}$$

and for small values of $b/\tau_{\rm aver}$ Eq. (7) becomes

$$\Upsilon(\tau_{\rm aver})=\Upsilon(\infty)+b''/\tau_{\rm aver}, \tag{9}$$

which explains the rectilinear behavior of Υ in Fig. 3. To determine the unbiased quantity $\Upsilon(\infty)$ we need to obtain $\Upsilon(\tau_{\rm aver})$ for a few values of $\tau_{\rm aver}$ and fit that data to one of the equations above.

E. Twist fluctuations in several directions

We have now discussed the use of twist fluctuations in a single direction and ordinary PBC in the two others. The

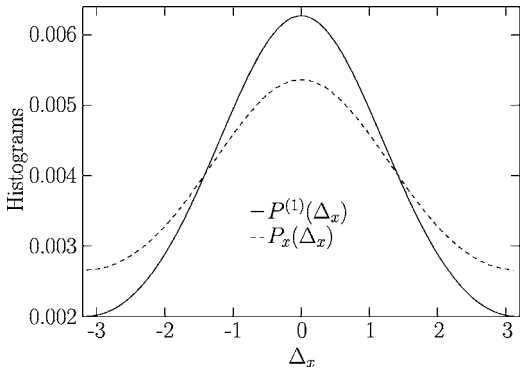

FIG. 4. A comparison of the twist histograms from simulations of the pure 3D *XY* model with twist fluctuations in one and three directions. The solid line is the distribution of Δ_x in simulations with $\Delta_y=\Delta_z=0$. The dashed line is the same quantity obtained with fluctuations in all three directions. The data are obtained from a cubic isotropic lattice with $L=8$ and $T=2.2$.

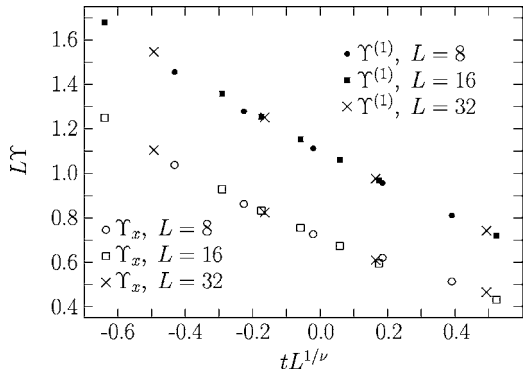

FIG. 5. The scaling collapse of the helicity modulii obtained in the pure 3D *XY* model. The upper symbols (solid) are the proper helicity modulus $\Upsilon^{(1)}$ obtained from Eq. (3) and the low symbols are for Υ_x obtained from $P_x(\Delta_x)$. The good collapse of the latter quantity confirms the expectation that it equally well may be used for examining the critical properties.

simulations of Ref. 15 were, however, done in a somewhat different way with twist fluctuations in all three directions. For this discussion we introduce the generalization $P^{(3)}(\Delta_x,\Delta_y,\Delta_z)$. With the phase angles of the *XY* model discretized to 256 different values, the computer memory needed to store such histograms rapidly becomes enormous. The collected histograms were therefore instead

$$P_x(\Delta_x)=\sum_{\Delta_y}\sum_{\Delta_z}P^{(3)}(\Delta_x,\Delta_y,\Delta_z),$$

and the analogous $P_y(\Delta_y)$ and $P_z(\Delta_z)$. For the quantity defined earlier with twist fluctuations in one dimension only we write,

$$P^{(1)}(\Delta_x)\equiv P^{(3)}(\Delta_x,0,0).$$

Figure 4 shows $P^{(1)}(\Delta_x)$ together with $P_x(\Delta_x)$. These two curves are very different and it becomes clear that the "helicity modulus" determined from P_x is not the same as the proper helicity modulus from the fluctuation formula or from $P^{(1)}$. However, from the universality hypothesis one would expect scaling of all kinds of quantities based on the free energy, and the similar behavior of Υ_x and $\Upsilon^{(1)}$ in Fig. 5 suggests that that actually is the case. Here we use the standard scaling assumption,

$$LY=f_Y(tL^{1/\nu}), \tag{10}$$

with the reduced temperature $t=(T/T_c-1)$.

F. Use in vortex glass simulations

As discussed above there are some complications in the determination of the helicity modulus from twist histograms. However, when our interest is only to determine the critical properties of a model, two of the above discussed complications may be disregarded. If the scaling hypothesis is phrased such that the properties of the free energy are a function only of the combination $tL^{1/\nu}$ it is clear that the precise method to examine these properties is not important as long as it is the same for all system sizes. Among other things this means that the choice of the range r of $P_\mu(\Delta_\mu)$ used for determining the helicity modulus is immaterial. Similarly, the difference between the proper helicity modulus and the quantity obtained from P_μ need not concern us either. The crucial point that has to be taken care of is the elimination of the bias of Sec. III D since this bias (as shown in Fig. 8) is different for different L.

When considering disordered systems there is one more point that should be taken under consideration. The parameter b in Eq. (7) has the dimension of time and may be interpreted as the time between two independent measurements. In a disordered system one expects the characteristic time to be different for different disorder realizations and one would need an average of a number of functions with different time constants. However, since the correction is linear in b, c.f. Eq. (9), such an average has the same functional form, but now with b as an *average* characteristic time.

IV. SIMULATION METHODS

A. The exchange steps

The exchange MC method—also called parallel tempering—is an elegant method that makes it possible to calculate the correct statistical averages in disordered systems where the usual MC methods would only be stuck in a local minimum. The idea is to simulate many different configurations in parallel and, beside the ordinary Metropolis MC steps, let the configurations perform a kind of constrained random walk in temperature space. These occasional changes in temperature mean that the configurations sometimes are at higher temperatures where the energy barriers between various local minima are low and easily may be overcome.

Our simulations were done with N_T temperatures, T_0 through T_{N_T-1}, chosen according to

$$T_m=T_{\min}\left(\frac{T_{\max}}{T_{\min}}\right)^{m/N_T},\quad m=0,\ldots,N_T-1. \tag{11}$$

The values of N_T, $T_{\min}$, and $T_{\max}$ as well as the number of disorder realizations and the length of the runs are detailed in Table II

TABLE II. The parameters describing the simulations. For systems of size $L\times L\times L_z$ we simulated N_d disorder configurations with N_T temperatures in the range $T_{\min}\leqslant T<T_{\max}$, cf. Eq. (11). Of the bins corresponding to $2^{18}=262\,144$ sweeps, $\tau_{\rm eq}$ are first discarded and the remaining $\tau_{\max}-\tau_{\rm eq}$ are used for calculating averages.

Data set	L	N_d	N_T	$T_{\min}$	$T_{\max}$	$\tau_{\rm eq}$	$\tau_{\max}$
A	10	600	12	0.09	0.24	1	16
$L_z/L=3/5$	15	600	24	0.09	0.24	4	16
	20	600	36	0.09	0.24	11	32
	25	200	36	0.115	0.24	17	48
A	10	900	12	0.09	0.24	2	13
$L_z/L=2/5$	15	900	24	0.09	0.24	5	17
	20	460	36	0.09	0.24	12	33
B	10	500	12	0.18	0.40	3	13
$L_z/L=1$	15	500	24	0.18	0.40	5	21
	20	300	36	0.18	0.40	7	21
C	8	400	8	0.16	0.38	1	12
$L_z/L=1$	12	700	16	0.16	0.38	2	15
	16	400	24	0.16	0.38	3	17
D	8	400	8	0.55	1.10	1	13
$L_z/L=1$	12	600	16	0.55	1.10	2	15
	16	600	24	0.55	1.10	3	17
	20	400	32	0.55	1.10	4	13

B. Check for equilibration

In spite of its beauty, the exchange MC method does not alleviate the need for thermalizing the system and it is therefore necessary to in some way monitor the approach to equilibrium. Since our main quantities from the simulations are the histograms $P_\mu(\Delta_\mu,\tau)$ we use these quantities in the analysis of the approach to equilibrium. The idea is to quantify the similarity of each histogram $P_\mu(\Delta_\mu,\tau)$ to the last histogram $P_\mu(\Delta_\mu,\tau_{\max})$, which is assumed to be typical of a thermalized system. The disorder averaged histogram difference is defined as

$$Q_\mu(\tau)=\left[\sum_{\Delta_\mu}|P_\mu(\Delta_\mu,\tau)-P_\mu(\Delta_\mu,\tau_{\max})|\right]_{\rm av}. \qquad (12)$$

The notation $[\ldots]_{\rm av}$ denotes the disorder averaging. $Q=1/2(Q_x+Q_y)$ is shown in Fig. 6 for $T=0.125$ (close to T_c) and our four system sizes. The larger values of $Q(\tau)$ for small τ mean that the histograms are more different from the thermalized system than at larger τ. This implies that the system is not yet thermalized and the number of bins needed to get down to the constant level of Q is the thermalization time ($\tau_{\rm eq}$ in Table II). These bins are skipped in the further analysis. The reason for the constant level of Q is the inevitable differences between histograms from different bins. For the larger systems the constant level of $Q(\tau)$ is rather large. However, to interpret the data correctly it should be kept in mind that the figure shows the difference between two histograms that both deviate from the true histogram of a hypothetical run of infinite length; the difference between a single histogram and the true one would give values that are roughly a factor of two smaller. The values nevertheless signal large fluctuations and convey a message about a complicated phase space with many different local minima.

The decrease of Q as $\tau\to\tau_{\max}$ is due to similarities between $P_\mu(\Delta_\mu,\tau\to\tau_{\max})$ and $P_\mu(\Delta_\mu,\tau_{\max})$ that are present because of the rather slow dynamics of the MC simulations. The total length of the simulations, $\tau_{\max}$, was chosen to get enough data for the extrapolation shown in Fig. 8.

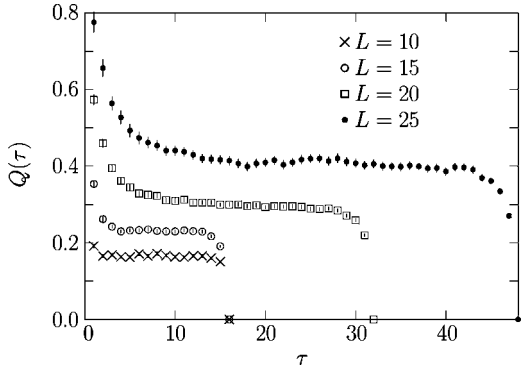

FIG. 6. The quantity $Q_\mu(\tau)$ is a disorder averaged measure of the difference between the histograms $P_\mu(\Delta_\mu,\tau)$ and $P_\mu(\Delta_\mu,\tau_{\max})$. The initial decrease down to a constant level shows the thermalization of the collection of N_T configurations. The decrease as $\tau\to\tau_{\max}$ is there because of correlations between $P_\mu(\Delta_\mu,\tau)$ for consecutive τ. This data is for set A with $L_z/L=3/5$; the shown quantity is $Q=1/2(Q_x+Q_y)$.

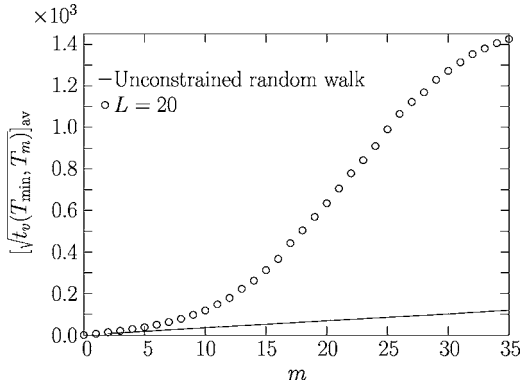

FIG. 7. The quantity $t_v(T_{\min}, T_m)$ is the time, measured in number of sweeps, for a configuration to travel from temperature T_m down to $T_{\min} \equiv T_{m=0}$. The open symbols show the disorder average of the square root of t_v based on 600 disorder configurations. The solid line is an estimate of the same quantity from the exchange acceptance. From the large difference it is clear that conclusions about the efficiency of the exchange steps to make the configurations travel across large temperature regions should not be drawn based on the acceptance ratio alone. We plot $\sqrt{t_v}$ since this quantity is proportional to the generalized distance for a simple random walk in the relevant phase space.

C. Efficiency of the exchange steps

A common way to monitor the efficiency of the exchange MC steps is to measure the exchange acceptance. This is, however, only a measure of the local mobility of the configurations and doesn't answer the more relevant question about the efficiency of the algorithm to move configurations across a larger temperature range. To keep track of all the exchange steps would mean producing an enormous amount of data and is therefore usually not convenient. A simple method has therefore been devised that gives the most relevant information with very little overhead. The idea is to, for each configuration, keep track of the time since the visit at each given temperature. To that end each configuration is accompanied by a vector of integers, v_m, with information about how long it was since the temperature T_m was last visited by that very configuration.

One way to use that information is to examine the vectors v_m for all configurations that were at the lowest temperature at the end of the run. A measure of the disorder averaged time since the last visit at temperature T_m is shown in Fig. 7. The same figure also shows the results from a simple simulation of an unconstrained random walk with the same properties and acceptance probability as in the exchange MC. As seen in the figure the difference is an order of magnitude, which indicates that conclusions about the efficiency of the exchange steps cannot be safely determined from the acceptance ratio alone. The reason for the long times needed for a configuration to travel from the highest to the lowest temperature is presumably that most high-temperature states are far away from the phase space regions typical of the lowest temperatures, which means that the configuration will usually have to undergo many thorough and time-consuming reorganizations before it can reach an energy compatible with the lowest temperatures.

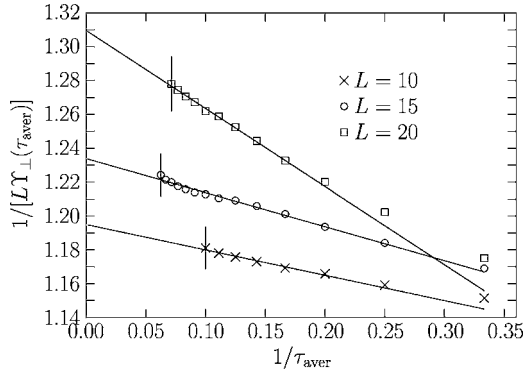

FIG. 8. The elimination of the bias in $\Upsilon_\perp(\tau_{\text{aver}})$ is done by extrapolating to $\tau_{\text{aver}} \to \infty$ with Eq. (8). The present data is from set B, $T=0.2685$ closely above T_c.

D. Eliminating the bias

For the following discussion we introduce a notation for the disorder averaged helicity modulii in the transverse and the parallel directions, respectively,

$$\Upsilon_\perp = \frac{1}{2}[\Upsilon_x + \Upsilon_y]_{\text{av}}, \tag{13a}$$

$$\Upsilon_\parallel = [\Upsilon_z]_{\text{av}}. \tag{13b}$$

The procedure used to determine the disorder averaged helicity modulus consists of three steps: (i) determine $\Upsilon_\mu(\tau_{\text{aver}})$ for each disorder configuration and several values of τ_{aver} by fitting histogram $\bar{P}_\mu(\Delta_\mu; \tau_{\text{aver}})$ based on τ_{aver} consecutive bins, $P_\mu(\Delta_\mu, \tau)$ to Eq. (4). (ii) Calculate the disorder averaged quantities $\Upsilon_\perp(\tau_{\text{aver}})$ and $\Upsilon_\parallel(\tau_{\text{aver}})$, cf. Eqs. (13). (iii) Fit this data to Eq. (8) to obtain the unbiased estimates $\Upsilon_\perp \equiv \Upsilon_\perp(\infty)$ and $\Upsilon_\parallel \equiv \Upsilon_\parallel(\infty)$. The last step is illustrated in Fig. 8. The error bars are the statistical errors associated with the disorder average for each size. It seems that the errors associated with the extrapolation to zero $1/\tau_{\text{aver}}$ are smaller than the errors due to the limited number of disorder realizations.

V. RESULTS

In this section we report the results from the analysis described above, with a number of different sets of parameters, cf. Table I. The purpose has been to explore the same model with a few different sets of parameters and to seek an overall consistency with 3D gauge glass universality rather than to try to achive the best possible precision on the exponent for a single set of parameters. Generally speaking that picture is confirmed, but the new simulations also give information about failure of finite size scaling for certain system sizes and parameters.

To properly specify the universality class one should determine two different exponents, e.g., ν that describes the growth of the correlations as $T \to T_c$ and η, which describes the correlations at T_c. An effect of twist fluctuations is to destroy some correlations and this makes it impossible to determine η. We do nevertheless consider the similar values

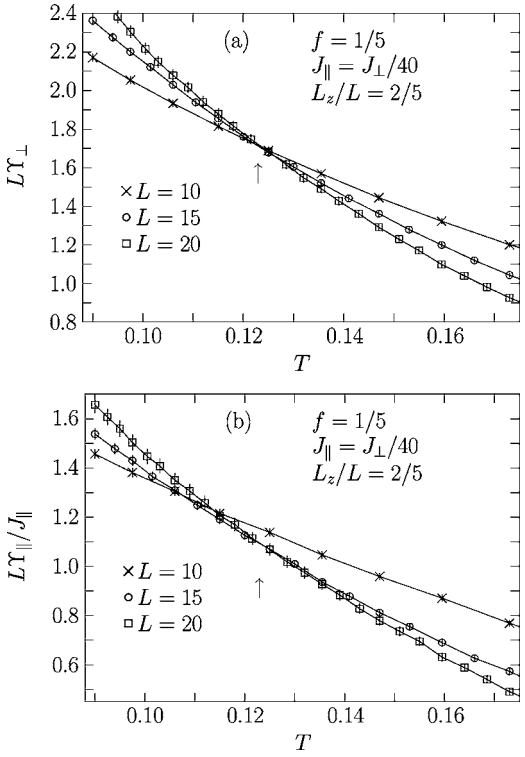

FIG. 9. Helicity modulii from simulations with aspect ratio $L_z/L=2/5$. The data for $LY_\perp$ in panel (a) all cross at $T_c \approx 0.123$ (shown by the arrow) in agreement with Ref. 15. Panel (b) for $LY_\parallel$ on the other hand shows the expected crossing only for the two largest sizes. The deviation from the scaling behavior is another example of the well-known fact that finite size scaling often fails for very small system sizes.

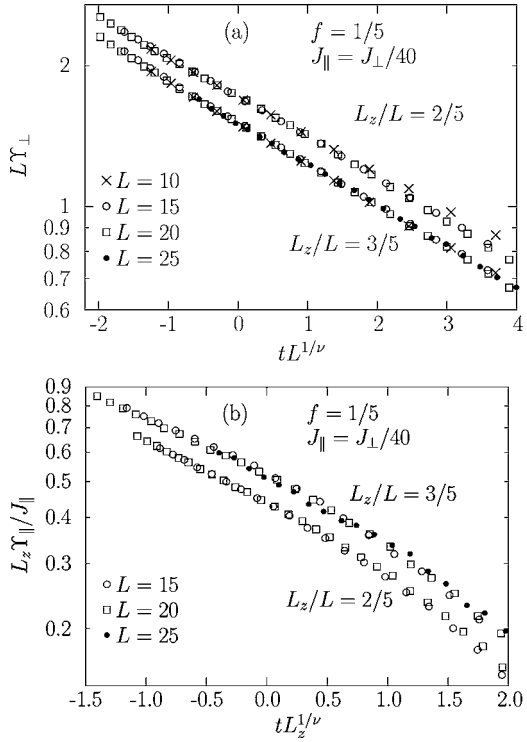

FIG. 10. Collapse of $LY_\perp$ and $L_z\Upsilon_\parallel$ with $\nu=1.5$ and $T_c=0.123$ from Ref. 15 for two different aspect ratios, $L_z/L=2/5$ and 3/5. The reduced temperature is $t=(T/T_c-1)$. For $\Upsilon_\parallel$ the data for the smallest size, $L=10$, has been omitted since it appears to be too small to scale, cf. panel (b) in Fig. 9.

of ν together with the *isotropic* scaling to give strong evidence for a common universality class.

A. High anisotropy, $J_\parallel/J_\perp=1/40$

The results in Ref. 15 were obtained with a rather high anisotropy, $J_\parallel/J_\perp=1/40$ and the aspect ratio $L_z/L=3/5$. We have now also performed simulations with a smaller aspect ratio, $L_z/L=2/5$, which is a good consistency test since not only the critical exponents but also the critical temperature should be independent of the aspect ratio. We have also performed additional simulations with several other aspect ratios to determine the anisotropy exponent.

1. Varying the aspect ratio

Figure 9 shows the helicity modulii for the same parameters as in Ref. 15 but with the aspect ratio $L_z/L=2/5$. We find a nice crossing for $LY_\perp$ at the expected value $T_c=0.123$.[15] The results for the perpendicular quantity $LY_\parallel$ also agree with this behavior for the two larger sizes but the data for the smallest system, $10\times10\times4$, is significantly off. This is in line with the general expectation that the scaling only should work for rather large system sizes. However, somewhat unexpectedly, the scaling in $LY_\perp$ prevails even though it fails in the direction parallel to the applied field.

Scaling collapses for the two aspect ratios $L_z/L=2/5$ and 3/5 are shown in Fig. 10. When discarding $\Upsilon_\parallel$ for $10\times10\times4$ the collapses with $T_c=0.123$ and $\nu=1.5$ (from Ref. 15) are excellent for both quantities. Note the similar shapes of the scaling functions for the two aspect ratios. For panel 10(b) this requires the use of L_z instead of L on the x axis. Also note that the dependency on the aspect ratio is the opposite for $L_z\Upsilon_\parallel$ compared to $LY_\perp$.

2. The anisotropy exponent

The above data is consistent with isotropic scaling, the anisotropy exponent $\zeta=1$, but to estimate the error bars we need a determination of the exponent. The idea behind finite size scaling is that certain quantities only should depend on the fraction ξ/L, and to generalize this concept to anisotropic scaling one has to allow for the possibility of two different correlation lengths, ξ and ξ_z, that grow in different ways as T_c is approached, $\xi_z \sim \xi^\zeta$. To do finite size scaling one needs sizes such that $\xi/L \propto \xi_z/L_z$ and with the above relation between ξ and ξ_z we need to determine the behavior of systems with $L_z \propto L^\zeta$. For general values of ζ this gives nonintegral L_z, and we obtain the appropriate data through interpolation of data for neighboring L_z-values. We have thus simulated with several different L_z: for $L=10$ we have used $L_z=5$, 6, and 7, and for $L=15$ simulations have been done with $L_z=8$, 9, and 10.

To determine limits on ζ the most straightforward test would be to repeat the scaling analysis with different values

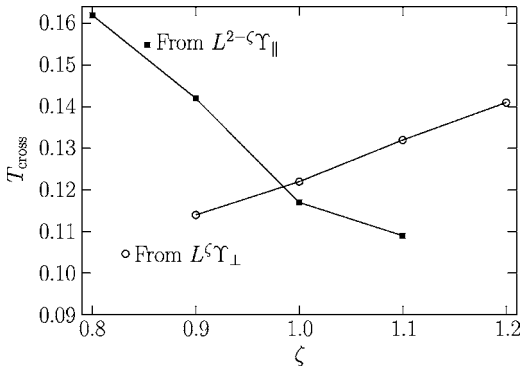

FIG. 11. The figure shows how the crossing temperature of $L^{\zeta}\Upsilon_\perp$ and $L^{2-\zeta}\Upsilon_\parallel$ with $L=15$ and $L=25$ depend on the assumed value of ζ. One set of data is for $(L,L_z)=(25,15)$ and the other for $(L,L_z)=(15,9\cdot(15/25)^{\zeta-1})$. The second set is obtained by interpolating the results from simulations with $L_z=8$, 9, and 10. Since a crossing of the data in both directions should occur at T_c, the correct value of ζ is obtained at the crossing of these two sets of data points. This gives $\zeta=1\pm0.1$, strongly suggestive of isotropic scaling.

of ζ and check how the quality of the scaling collapse depends on ζ. Because of the statistical errors in the raw data, however, that is not a very useful technique. A more sensitive test is obtained by combining results from analyses of both $\Upsilon_\perp$ and $\Upsilon_\parallel$. To do that we focus on how the crossing temperatures of $L^{\zeta}\Upsilon_\perp$ and $L^{2-\zeta}\Upsilon_\parallel$ depend on ζ. To make the test clean and simple we only make use of two sizes at the time. Figure 11 shows the dependency of the crossing temperatures on ζ for sizes $L=15$ and 25. The two different crossing temperatures coincide at $T\approx0.12$ and $\zeta\approx1$. Note that the two quantities have the opposite dependency on ζ. This is the key to this more precise determination of ζ, and together with a rough error estimate Fig. 11 gives $\zeta=1\pm0.1$.

B. Less anisotropic, $J_\parallel/J_\perp=1/10$

The simulations discussed in the previous section are for a rather strong anisotropy, $J_\parallel/J_\perp=1/40$. It is generally expected that the critical behavior should be independent of details as the anisotropy, and we now check this expectation with simulations for $J_\parallel/J_\perp=1/10$; data sets B and C in Table I. Figure 12 shows scaling collapses of the helicity modulii for data set B. Beside the weaker anisotropy the simulations also differ in that the disorder $\varepsilon_{i\mu}$ is stronger and is now chosen from a uniform rectangular distribution between -1 and 1, corresponding to $p=\sqrt{\langle\varepsilon_{ij}^2\rangle}=1/\sqrt{3}\approx0.577$. In a fit with T_c and ν as adjustable parameters a collapse of $L\Upsilon_\perp$ gives $T_c=0.238$ and $\nu=1.57$ whereas a collapse of $L\Upsilon_\parallel$ gives $T_c=0.241$ and $\nu=1.98$. The different values of ν are an indication of the rather low precision in these determinations. In Fig. 12 we show that it is possible to collapse both sets of data with the same parameters, $T_c=0.24$ and $\nu=1.6$. The collapse of $L\Upsilon_\perp$ is very nice whereas the collapse of $L\Upsilon_\parallel$, especially in a region around T_c, is somewhat worse. However, considering the statistical errors, we believe this to be just a statistical fluctuation. The fact that several points around T_c all deviate in the same way is an artifact of the exchange

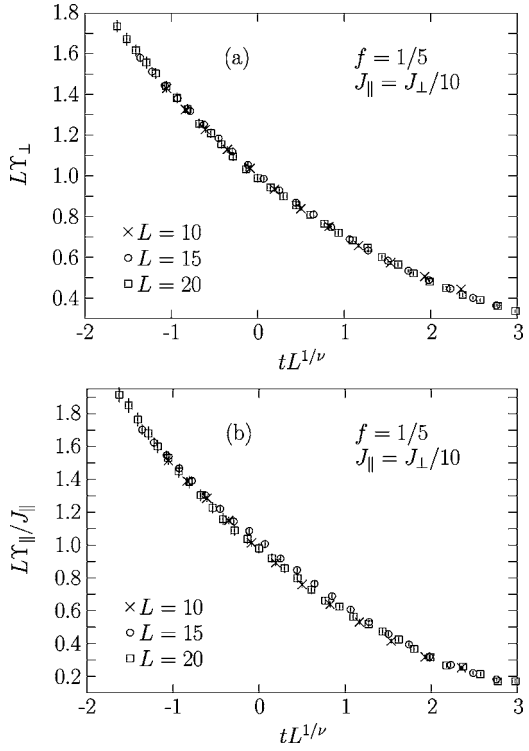

FIG. 12. The data collapse for $f=1/5$ and $J_\parallel/J_\perp=1/10$. The collapse is done with the same $T_c=0.24$ and $\nu=1.6$ for both data sets to demonstrate that both quantities may be collapsed with the same parameters.

Monte Carlo method since the exchange steps have the effect to give correlations between results at neighboring temperatures.

We have also simulated data set C in Table I with the same anisotropy but with the filling factor $f=1/4$. The collapse which is found in Fig. 13 is excellent and we obtain $\nu=1.35$ and $\nu=1.48$ from the scaling collapses of $L\Upsilon_\perp$ and $L\Upsilon_\parallel$, respectively.

C. Isotropic system

The values for ν given above, obtained from simulations with different values of anisotropy and filling factor, are within reasonable error bars consistent with 3D gauge glass universality, $\nu\approx1.39$. This seems to rule out the possibility that the nice scaling in Ref. 15 was only a coincidence. Still, the results presented in the present section show that scaling fails when the analysis is applied to an isotropic model. This finding is of some importance since isotropic couplings have been used in several investigations[12–14] of vortex glass models. These papers reach differing conclusions and we believe that an understanding of the problem of scaling our data from isotropic couplings may shed some light on problems in these investigations.

1. Failure to scale the data

For simulations of an isotropic system we use the same parameters as Kawamura in Ref. 13 but the analysis differs from theirs in that we focus on the behavior of the helicity

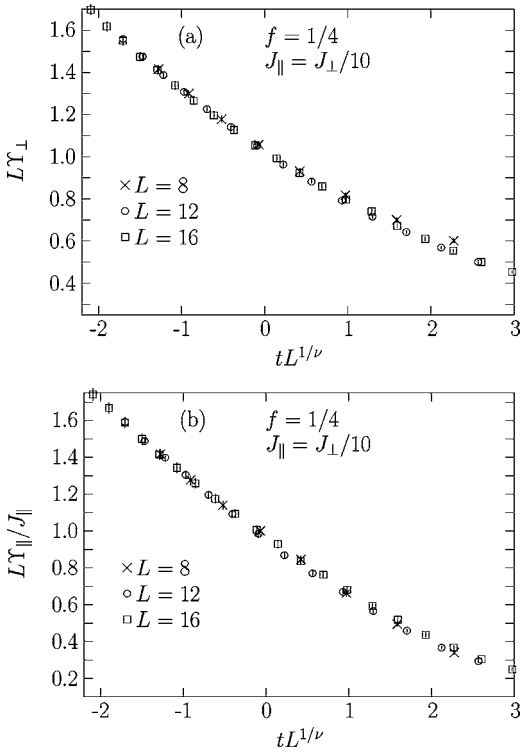

FIG. 13. The data collapse of $L\Upsilon_\perp$ and $L\Upsilon_\parallel$ for $f=1/4$ and $J_\parallel/J_\perp=0.1$. The parameters used in the data collapses are $\nu=1.4$ and $T_c=0.225$.

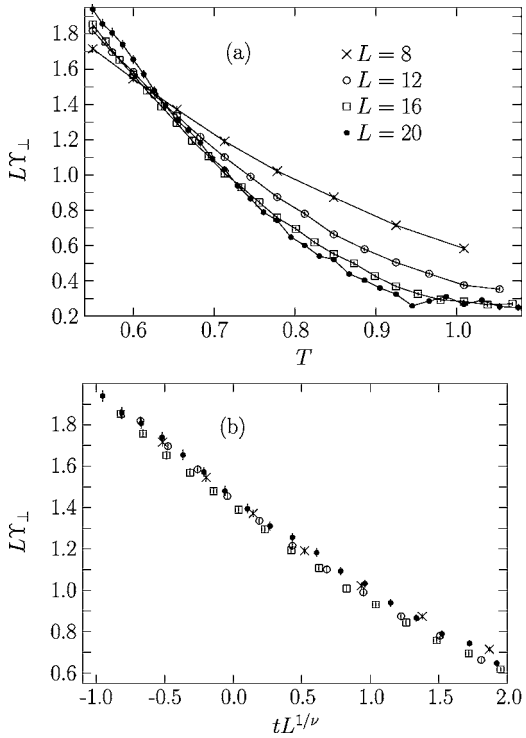

FIG. 14. The raw data and attempted data collapse of $L\Upsilon_\perp$ for the isotropic system with $f=1/4$. The parameters in the data collapse in panel (b) are $\nu=1.50$ and $T_c=0.63$. The value of the exponent is consistent with $\nu\approx 1.39$ in the 3D gauge glass, but the quality of the collapse is not satisfactory.

modulii instead of the root-mean-square (rms) current.

Figure 14(a) shows $L\Upsilon_\perp$ for the four system sizes $L=8$, 12, 16, and 20. The data for $L\Upsilon_\perp$ weakly suggests the possibility of scaling and panel 14(b) shows the attempted scaling collapse with $T_c\approx 0.63$ and $\nu\approx 1.50$. Even though the value of ν is in good agreement with our earlier findings, the poor quality of the collapse makes it impossible to draw any more definite conclusions. Turning to $L\Upsilon_\parallel/J_\parallel$ shown in Fig. 15, we find that it is impossible to collapse the data since the crossing points for two successive system sizes shift systematically to lower temperatures for increasing L. Beside the failure to scale the data it should be noted that $L\Upsilon_\parallel/J_\parallel$ for the isotropic case is exceptionally large. For all the other cases we had $L\Upsilon_\parallel/J_\parallel\approx 1.0$ at T_c, but in the isotropic model, this quantity is considerably larger in the temperature region of interest.

2. The reason for the failure to scale

The behavior of $\Upsilon_\parallel$ in the isotropic system is thus clearly different from the anisotropic systems with $J_\parallel/J_\perp=1/40$ or $1/10$. We will now argue that this is because the disorder in the coupling constants is not effective in fully disordering the system for the accessible system sizes.

As a probe of the loss of order we use Δ_μ^0, which is the position of the minimum of the free energy, $F_\mu(\Delta_\mu)$. This quantity has been used before as a measure of the effective strength of the disorder.[28] The disorder fixed point was characterized by $\langle|\Delta_\mu^0|\rangle=\pi/2$, which corresponds to a uniform distribution between $-\pi$ and π. Figure 16 shows histograms of Δ_z^0 and Δ_x^0 from our data and it is clear that the histograms are very different from a uniform distribution. Especially the histograms of Δ_z^0 are very narrow with $|\Delta_z^0/\pi|<0.1$ for almost 99% of the disorder realizations. For Δ_x^0 the distributions are considerably wider but are still clearly peaked around zero. In both cases there is some finite size dependence, with a wider distribution for larger system sizes. For comparison we also show the corresponding histograms for the anisotropic model with $J_\parallel/J_\perp=1/10$ in Fig. 17. For the anisotropic case the histograms of $\Delta_{x,z}^0$ are close to a uniform

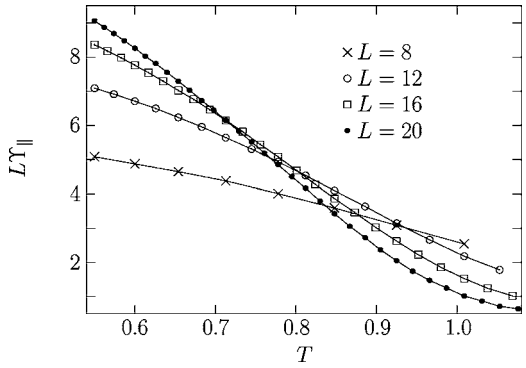

FIG. 15. The raw data of $L\Upsilon_\parallel$ for the isotropic system with $f=1/4$. Since the crossing temperature for two successive sizes shift systematically with increasing L it is impossible to collapse the data. The large magnitude of $L\Upsilon_\parallel$ gives additional evidence that the isotropic system is different from the anisotropic ones.

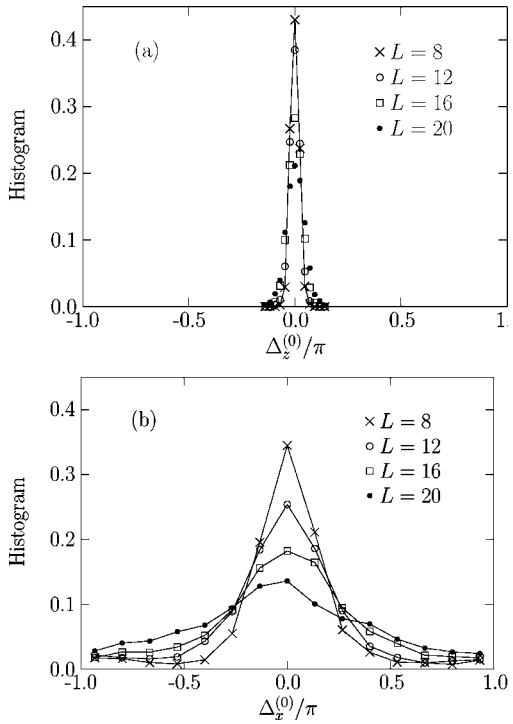

FIG. 16. The histograms of Δ_z^0 and Δ_x^0 for the isotropic system with $f=1/4$. In a fully disordered system one expects Δ_μ^0 to be uniformly distributed between $-\pi$ and π, but the figure shows that that is not the case for $J_\parallel=J_\perp$. The peak around zero is strongest for Δ_z^0 in panel (a) but is also very clear for Δ_x^0 in panel (b). The histograms are calculated on the basis of data for all the simulated temperatures.

distribution; only the data for $L=8$ have somewhat more weight around zero. This shows that the data that exhibits good scaling are from strongly disordered systems. In contrast, the isotropic model appears to be far from the disorder fixed point and we believe that this is at the root of the failure to find a convincing data collapse.

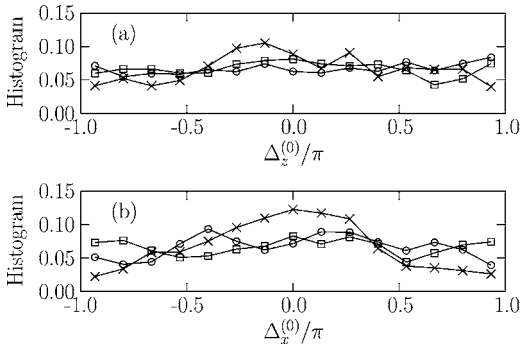

FIG. 17. The figures show histograms of Δ_z^0 and Δ_x^0 for anisotropy $J_\parallel/J_\perp=1/10$ and $f=1/4$ in panel (a) and panel (b), respectively. The results for the larger sizes, $L=12$ and 16 (circles and squares), are consistent with a uniform distribution whereas the distributions for $L=8$ (crosses) have somewhat more weight around zero. However, it seems that such small deviations from perfect disorder (a flat histogram) have no discernible effects on the scaling shown in Fig. 13. The histograms are calculated on the basis of data for all the simulated temperatures.

To discuss the physical meaning of Δ_μ^0 we return to Fig. 2, which illustrates the relation between the size of a vortex pair and the value of the twist variable in the direction perpendicular to the separation. As the pair separates in the x direction the twist Δ_y gradually increases. At zero temperature the twist is to a good approximation proportional to the distance, d, between the vortices, $\Delta_y=2\pi d/L$. For the more general situation with several vortices the vortex separation generalizes to the total dipole moment of the system of vortices, $p_x=\Sigma_i x_i q_i$, where i enumerates the vortices, x_i is the x-coordinate of vortex i, and q_i is the vorticity (charge). At nonzero T the distribution of Δ_y at constant p_x will be wider; the relevant expressions are given in Ref. 29. For the three-dimensional case the dipole moment generalizes to the projection of the vortex loops on a certain plane, C^{xy}.[30] The corresponding relation is then $\Delta_z=2\pi C^{xy}/L^2$.

In a pure system the twist histogram will always be symmetric around zero, $\Delta_\mu^0=0$, but the effect of the disorder is to favor certain vortex loops between the layers and suppress others. The net effect may be a nonzero C^{xy} and accordingly a shift of Δ_z^0 away from zero. Our interpretation of the results in Fig. 16 is therefore that the disorder is not strong enough to introduce loops between the layers. Note that field-induced vortex lines that have a nonvanishing projection on the x-y plane also contribute to C^{xy}. The absence of large disorder-introduced vortex loops between the layers (or the equivalent deflection of the field-induced vortex lines) means that Δ_z^0 is always close to zero.

The analyses above suggests that a strong coupling in the field direction has the effect to reduce the amount of disorder-induced vortex loops between the planes. The effect is to get Δ^0 close to zero which means that the effective disorder is small in the system and we believe that this is responsible for the failure of the helicity modulii to scale. Considering the broadening of the histograms with increasing L in Fig. 16, we expect this to be a finite size effect, but are presently unable to estimate the size where scaling could be expected to set in.

VI. DISCUSSION

The use of an anisotropic model in the study of critical phenomena with finite size scaling deserves some comments. To get data with high precision for finite size scaling from Monte Carlo simulations, the correlation volume should ideally have the same shape as the simulation cell. In an isotropic model a cubic simulation cell is therefore the best choice and in the general case one wants a common value of the fraction ξ_μ/L_μ in all directions. For the model in the present paper with a symmetry breaking field there is nothing that guarantees that isotropic couplings are best. It is, however, possible to extract some information about the correlations from the helicity modulii. With Υ_μ as the measure of the phase coherence, a larger Υ_μ implies stronger correlations across the system and thereby a larger fraction ξ_μ/L_μ. By comparing data for the isotropic model in Figs. 14 and 15, the fact that $\Upsilon_\parallel$ is considerably larger than $\Upsilon_\perp$ leads us to conclude that the correlations across the system are considerably stronger in the field direction compared to the perpen-

dicular direction. One way to reach the goal of a simulation cell with the same shape as the correlation volume would then be to increase the aspect ratio L_z/L, but a different and more efficient way is to instead decrease $J_\parallel$, the coupling strength in the field direction.

To get a better understanding of the effect of anisotropic couplings on the helicity modulii we have made some additional simulations on the ordinary 3D *XY* model (zero field and no disorder) with $J_z/J=1/4$. Since one expects $\xi_\mu \propto \sqrt{J_\mu}$ the aspect ratio was chosen as $L_z/L=1/2$ to give a simulation cell with the same shape as the correlation volume. With this value of the aspect ratio the simulations give $\Upsilon/J=\Upsilon_z/J_z$ at T_c to a good approximation. As shown in Fig. 12 the same relation holds to a good approximation at and close to T_c in the simulations of the vortex glass with $J_\parallel/J_\perp=1/10$ and $L_z/L=1$. This suggests that the correlations in the different directions are about equally strong when the anisotropy is set to $J_\parallel/J_\perp=1/10$ and that this value therefore is close to optimal for the anisotropy in the vortex glass simulations with $f=1/5$.

Even though it thus seems that our model is best examined with a rather large anisotropy we now turn to the results obtained with isotropic couplings. These simulations were performed with the parameters of Ref. 13 to facilitate a direction comparison. It is, however, clear that our results are significantly different from what was reported there. Whereas our $L\Upsilon_\perp$ almost collapse at $T=0.63$ with $\nu \approx 1.5$ their corresponding quantity, I_T, collapses for the three largest sizes at $T_g=0.81$ with $\nu=1.0$. Especially the different values of the critical temperature points to a systematic difference.

We believe that the reason for this difference is the calculation of I_T from the derivative of $F(\Delta)$ evaluated at $\Delta=0$ (see Ref. 13), rather than at random values of Δ. To analyze the vortex glass transition the question to examine is whether the free energy $F(\Delta)$ becomes flat or rough in the limit of large L. One may then make use of any quantity that gives a good measure of the amount of structure in $F(\Delta)$ and examine how this quantity changes with increasing L. Two such quantites are $d^2F/d\Delta^2$ evaluated at the minimum of $F(\Delta)$ and $dF/d\Delta$ evaluated at a random Δ. In the 3D gauge glass, where the randomness is put in the vector potential A_{ij}, a random Δ may be absorbed into the similarly random A_{ij} and it is then acceptable to determine the root-mean-square current $I_{\rm rms}$ at $\Delta=0$. Or, to put it differently, the evaluation at $\Delta=0$ is acceptable since the structure in $F(\Delta)$ is spread uniformly across the entire interval of Δ.

For the isotropic system with $f=1/4$ (parameter set D) it was shown in Fig. 16 that the structure in $F_\mu(\Delta_\mu)$ is not spread uniformly across Δ; the minima Δ^0_μ are mostly at values close to zero, and we conclude that it is not safe to evaluate the current at $\Delta=0$. To further explore this effect we have examined the data for isotropic couplings. It was then found that the typical structure of $F(\Delta_\mu)$ is a single minimum with a shape that to a very good approximation is parabolic, $F(\Delta_\mu)=\text{const}+L\Upsilon_\mu(\Delta_\mu-\Delta^0_\mu)^2/2$, where both Υ_μ and Δ^0_μ vary with disorder realization. When the derivative is evaluated at $\Delta_\mu=0$ one then gets $I_\mu=-L\Upsilon_\mu\Delta^0_\mu$, and the disorder averaged quantity becomes

$$I^2_{\rm rms}=[(L\Upsilon_\mu\Delta^0_\mu)^2]_{\rm av}.$$

This shows that a size-dependence in the distribution of Δ^0_μ (as in Fig. 16) will affect $I_{\rm rms}$. If there is a temperature where $L\Upsilon_\mu$ is independent of L, then $I_{\rm rms}$ will be an increasing function of L due to the size-dependence of the distribution of Δ^0_μ. We believe this to be the reason for the different critical behavior in Ref. 13 compared to the results in the present paper.

The failure of the helicity modulus to scale in the isotropic model is a related but different question. As discussed in Sec. V C 2 a message from Fig. 16 is that the isotropic model is not sufficiently disordered for the simulated system sizes and it seems possible that this remaining order destroys the transition. The broadening of the histograms in Fig. 16 with increasing system size would eventually lead to a uniform distribution and one would then expect scaling with the 3D gauge glass exponents. However, considering the slow widening of the histograms as L increases, scaling would presumably only be seen for very large systems.

To summarize, the main conclusion of the present investigation is that data from the vortex glass model with several different sets of parameters may be nicely collapsed with isotropic scaling ($\zeta=1$) and values for the correlation length exponent consistent with 3D gauge glass universality. This is a confirmation of the behavior found in Ref. 15. Still, it is found that data from simulations with isotropic couplings do not give any convincing scaling collapse and we argue that the reason is that the effective randomness for the accessible system sizes is too small to give the correct behavior of the vortex glass transition.

ACKNOWLEDGEMENTS

We acknowledge discussions with S. Teitel. This work was supported by the Swedish Research Council, Contract No. 2002-3975, and by the resources of the Swedish High Performance Computing Center North (HPC2N).

[1] M. P. A. Fisher, Phys. Rev. Lett. **62**, 1415 (1989).
[2] D. S. Fisher, M. P. A. Fisher, and D. A. Huse, Phys. Rev. B **43**, 130 (1991).
[3] P. L. Gammel, L. F. Schneemeyer, and D. J. Bishop, Phys. Rev. Lett. **66**, 953 (1991).
[4] T. Klein, A. Conde-Gallardo, J. Marcus, C. Escribe-Filippini, P. Samuely, P. Szabó, and A. G. M. Jansen, Phys. Rev. B **58**, 12411 (1998).
[5] A. M. Petrean, L. M. Paulius, W.-K. Kwok, J. A. Fendrich, and G. W. Crabtree, Phys. Rev. Lett. **84**, 5852 (2000).
[6] C. Reichhardt, A. van Otterlo, and G. T. Zimányi, Phys. Rev. Lett. **84**, 1994 (2000), and references therein.

[7] D. A. Huse and H. S. Seung, Phys. Rev. B **42**, R1059 (1990).
[8] J. D. Reger, T. A. Tokuyasu, A. P. Young, and M. P. A. Fisher, Phys. Rev. B **44**, R7147 (1991).
[9] K. Hukushima and K. Nemoto, J. Phys. Soc. Jpn. **65**, 1604 (1996).
[10] H. G. Katzgraber and I. A. Campbell, Phys. Rev. B **69**, 094413 (2004).
[11] M. J. P. Gingras, Phys. Rev. B **45**, 7547 (1992).
[12] H. Kawamura, J. Phys. Soc. Jpn. **69**, 29 (2000).
[13] H. Kawamura, Phys. Rev. B **68**, 220502(R) (2003).
[14] A. Vestergren, J. Lidmar, and M. Wallin, Phys. Rev. Lett. **88**, 117004 (2002).
[15] P. Olsson, Phys. Rev. Lett. **91**, 077002 (2003).
[16] X. Hu, S. Miyashita, and M. Tachiki, Phys. Rev. Lett. **79**, 3498 (1997).
[17] P. Olsson and S. Teitel, Phys. Rev. Lett. **82**, 2183 (1999).
[18] J. Lidmar, Phys. Rev. Lett. **91**, 097001 (2003).
[19] P. Olsson and S. Teitel, Phys. Rev. Lett. **87**, 137001 (2001).
[20] P. Olsson, Phys. Rev. B **52**, 4511 (1995).
[21] The splitting up of Δ_μ in L_μ different variables has been done for technical reasons. With the angles θ_i discretized to 250 different values (divisible by $1/f=5$) the minimum change of δ_μ (as a single variable) would for a system with $L_\mu=25$ give changes of Δ_μ as large as 25/250. This would lead to only ten different values of Δ_μ. By instead using L_μ different variables $\delta_\mu^{(\mathbf{r}_i\cdot\hat{\mu})}$ the sum Δ_μ may take on all the possible values.
[22] P. Olsson and S. Teitel (unpublished).
[23] S. Teitel and C. Jayaprakash, Phys. Rev. B **27**, 598 (1983).
[24] J. M. Thijssen and H. J. F. Knops, Phys. Rev. B **37**, 7738 (1988).
[25] P. Olsson, Phys. Rev. B **46**, 14598 (1992).
[26] A. Vallat and H. Beck, Phys. Rev. B **50**, 4015 (1994).
[27] U. Wolff, Phys. Rev. Lett. **62**, 361 (1989).
[28] J. M. Kosterlitz and M. V. Simkin, Phys. Rev. Lett. **79**, 1098 (1997).
[29] P. Gupta, S. Teitel, and M. J. P. Gingras, Phys. Rev. Lett. **80**, 105 (1998).
[30] H. S. Bokil and A. P. Young, Phys. Rev. Lett. **74**, 3021 (1995).